

**OPEN ACCESS**

# Nanostructured Coating for Aluminum Alloys Used in Aerospace Applications

To cite this article: Maido Merisalu *et al* 2022 *J. Electrochem. Soc.* **169** 071503

View the [article online](#) for updates and enhancements.



## ECS Membership = Connection

### ECS membership connects you to the electrochemical community:

- Facilitate your research and discovery through ECS meetings which convene scientists from around the world;
- Access professional support through your lifetime career;
- Open up mentorship opportunities across the stages of your career;
- Build relationships that nurture partnership, teamwork—and success!

**Join ECS!**

**Visit [electrochem.org/join](https://electrochem.org/join)**





## Nanostructured Coating for Aluminum Alloys Used in Aerospace Applications

Maido Merisalu,<sup>1</sup> Lauri Aarik,<sup>1</sup>  Helle-Mai Piirsoo,<sup>1</sup> Jekaterina Kozlova,<sup>1</sup>  Aivar Tarre,<sup>1</sup>  Roberts Zabels,<sup>2</sup> Johanna Wessing,<sup>3</sup> Abel Brieva,<sup>3</sup> and Väino Sammelselg<sup>1,2</sup> 

<sup>1</sup>University of Tartu, Institute of Physics, 50411 Tartu, Estonia

<sup>2</sup>University of Latvia, Institute of Solid State Physics, LV-1063 Riga, Latvia

<sup>3</sup>European Space Agency, European Space Research and Technology Centre, 2201 AZ Noordwijk, Netherlands

A thin industrial corrosion-protection nanostructured coating for the Al alloy AA2024-T3 is demonstrated. The coating is prepared in a two-step process utilizing hard anodizing as a pre-treatment, followed by sealing and coating by atomic layer deposition (ALD). In the first step, anodizing in sulfuric acid at a low temperature converts the alloy surface into a low-porosity anodic oxide. In the second step, the pores are sealed and coated by low-temperature ALD using different metal oxides. The resulting nanostructured ceramic coatings are thoroughly characterized by cross-sectioning using a focused ion beam, followed by scanning electron microscopy, transmission electron microscopy, X-ray microanalysis, and nanoindentation and are tested via linear sweep voltammetry, electrochemical impedance spectroscopy, salt spray, and energetic atomic oxygen flow. The best thin corrosion protection coating, made by anodizing at 20 V, 1 °C and sealing and coating with amorphous Al<sub>2</sub>O<sub>3</sub>/TiO<sub>2</sub> nanolaminate, exhibits no signs of corrosion after a 1000 h ISO 9227 salt spray test and demonstrates a maximum surface hardness of 5.5 GPa. The same coating also suffers negligible damage in an atomic oxygen test, which is comparable to 1 year of exposure to space in low Earth orbit.

© 2022 The Author(s). Published on behalf of The Electrochemical Society by IOP Publishing Limited. This is an open access article distributed under the terms of the Creative Commons Attribution 4.0 License (CC BY, <http://creativecommons.org/licenses/by/4.0/>), which permits unrestricted reuse of the work in any medium, provided the original work is properly cited. [DOI: 10.1149/1945-7111/ac7bb2]



Manuscript submitted April 30, 2022; revised manuscript received June 22, 2022. Published July 1, 2022.

Supplementary material for this article is available [online](#)

Aluminum alloys of the AA2000 series, such as AA2024-T3, are favored for automobile, drone, and aerospace applications because of their light weight, high strength, and adequate workability.<sup>1–5</sup> The latter alloy has an elemental composition, phase structure, and vulnerability to localized pitting corrosion that are very similar to those of AA2219-T851, which is used for structural components of the International Space Station, outer-space rovers, and satellites.<sup>6,7</sup> The use of lightweight materials for the manufacture of structural parts for the applications mentioned above minimizes the consumption of fuel or energy stored in batteries, which expands the operation time of vehicles, reduces the carbon footprint from the use of fossil-based fuels, and minimizes the emission of greenhouse gases. The latter applies to both fossil fuels and hydrogen, which contribute to global warming in different ways. For instance, CO<sub>2</sub> and water vapor are both potent greenhouse gases (GHGs) and are formed from the combustion of fossil fuels and hydrogen, respectively. Furthermore, hydrogen is mostly produced via steam methane reforming, which is cost-effective but generates significant CO<sub>2</sub> emissions.<sup>8</sup> Aluminum alloys are also widely used for satellite construction for several reasons. The light weight of the alloys minimizes the total mass of the satellite and, therefore, the cost of shipping it into orbit.<sup>9</sup> The low atomic number of aluminum makes it also a good radiation shielding material because its interaction with high-energy cosmic radiation results in less harmful secondary electromagnetic radiation than higher atomic number materials such as steels.<sup>10</sup> Furthermore, aluminum alloys exhibit excellent electrical conductivity, which is useful for thermal regulation, as well as for mitigating the charging of surfaces due to cosmic radiation.

The benefits of using aluminum alloys are clear; however, these metals suffer from distinct problems in their application environments. For instance, the presence of humidity and chloride ions in terrestrial applications and even aboard space stations may cause galvanic corrosion, which is promoted by other passive metals in electrical contact with the primary aluminum component as well as by different types of near-surface intermetallic particles.<sup>11–14</sup> In space applications, however, connected metal parts may get stuck owing to cold welding, which is particularly problematic for

components that need to retain their mobility (e.g., mechanical scanning mechanisms).<sup>15</sup> The problem of cold welding may be further enhanced by fretting, which is caused by vibration during launch or by movement of antennas in space. A possible example of this phenomenon is a bolt that became stuck on the Hubble Space Telescope, hindering the maintenance of the expensive instrument.<sup>16</sup> However, in this case, corrosion caused by atomic oxygen<sup>17,18</sup> may have also played a role, causing corrosion products to build up around the threads of the bolt over time.

The aforementioned problems with aluminum alloys can be mitigated with different types of functional coatings depending on the dimensional tolerance, shape, and purpose of the component. In particular, for coating substrates with sophisticated three-dimensional shapes, there are currently three distinct methods that cover different thickness ranges: anodizing,<sup>19,20</sup> plasma electrolytic oxidation (PEO),<sup>15,21</sup> and atomic layer deposition.<sup>22–28</sup> During anodization, the top layer of the aluminum alloy is electrochemically converted into porous anodic aluminum oxide (AAO), which normally has a thickness ranging from tens of micrometers to several millimeters.<sup>19,20</sup> After anodizing, the AAO layer needs to be sealed to gain improved resistance against corrosion and wear or to alter other properties of the surface, such as its optical properties. The PEO process is performed in mildly alkaline electrolytes and at higher potentials than anodizing, which causes discharge at the alloy-electrolyte interface.<sup>15,21</sup> The high temperature at discharge causes the obtained oxide layer to be partially crystalline, which increases its overall hardness. Optimized PEO processes can therefore be used to create oxide layers that are tens of microns thick and outperform the coatings obtained via anodization, particularly at the lower end of the thickness range. Overall, both anodizing and PEO can be used to protect aluminum components against wear and corrosion, but also to prevent cold welding of parts in space. In contrast to anodizing and PEO, ALD allows the preparation of the thinnest protective coatings, which are as a rule ≤100 nm thick, see overviews in earlier works.<sup>23,27</sup> Unfortunately, these coatings provide only limited corrosion protection.<sup>23,24</sup> Even the best performing nanolaminates containing Al<sub>2</sub>O<sub>3</sub> and TiO<sub>2</sub> layers, and being deposited directly onto the alloy surface, fail at characteristic sites, where the failure mechanism is most likely related to near-surface intermetallic particles.<sup>12,27</sup> In our previous studies, we also showed that electrochemical pre-treatments enhance the performance of coatings made by ALD and potentially even allow the preparation

<sup>7</sup>E-mail: [vaino.sammelselg@ut.ee](mailto:vaino.sammelselg@ut.ee)

of a new type of high-performance nanostructured coating by sealing the AAO layer with different ceramic materials.<sup>25,27,28</sup> If the approach can be scaled up in a practical manner, then such nanostructured coatings may be able to occupy the 0.1–5  $\mu\text{m}$  thickness range, which is particularly lucrative for precision components in high-performance applications, where excellent resistance to corrosion and wear are required.

The aforementioned problems with aluminum alloys can be mitigated with different types of functional coatings depending on the dimensional tolerance, shape, and purpose of the component. In particular, for coating substrates with sophisticated three-dimensional shapes, there are currently three distinct methods that cover different thickness ranges: anodizing,<sup>19,20</sup> plasma electrolytic oxidation (PEO),<sup>15,21</sup> and atomic layer deposition.<sup>22–28</sup> During anodization, the top layer of the aluminum alloy is electrochemically converted into porous anodic aluminum oxide, which normally has a thickness ranging from tens of micrometers to several millimeters.<sup>19,20</sup> After anodizing, the AAO layer needs to be sealed to gain improved resistance against corrosion and wear or to alter other properties of the surface, such as its optical properties. The PEO process is performed in mildly alkaline electrolytes and at higher potentials than anodizing, which causes discharge at the alloy-electrolyte interface.<sup>15,21</sup> The high temperature at discharge causes the obtained oxide layer to be partially crystalline, which increases its overall hardness. Optimized PEO processes can therefore be used to create oxide layers that are tens of microns thick and outperform the coatings obtained via anodization, particularly at the lower end of the thickness range. Overall, both anodizing and PEO can be used to protect aluminum components against wear and corrosion, but also to prevent cold welding of parts in space. In contrast to anodizing and PEO, ALD allows the preparation of the thinnest protective coatings, which are as a rule  $\leq 100$  nm thick, see overviews in earlier works.<sup>23,27</sup> Unfortunately, these coatings provide only limited corrosion protection.<sup>23,24</sup> Even the best performing nanolaminates containing  $\text{Al}_2\text{O}_3$  and  $\text{TiO}_2$  layers, and being deposited directly onto the alloy surface, fail at characteristic sites, where the failure mechanism is most likely related to near-surface intermetallic particles.<sup>12,27</sup> In our previous studies, we also showed that electrochemical pre-treatments enhance the performance of coatings made by ALD and potentially even allow the preparation of a new type of high-performance nanostructured coating by sealing the AAO layer with different ceramic materials.<sup>25,27,28</sup> If the approach can be scaled up in a practical manner, then such nanostructured coatings may be able to occupy the 0.1–5  $\mu\text{m}$  thickness range, which is particularly lucrative for precision components in high-performance applications, where excellent resistance to corrosion and wear are required.

## Experimental

**Pre-treatment of the substrates.**—AA2024-T3 (Al alloy) alclad plates (Goodfellow) with dimensions of  $20 \times 20 \text{ mm}^2$  (smaller) and  $40 \times 110 \text{ mm}^2$  (larger) samples were used in most of the experiments, with the Al cladding mechanically removed from the original 3 mm sheet by machine milling. The thickness of the plates after milling was  $2.6 \pm 0.2$  mm. The standard composition of the alloy<sup>5</sup> is listed in Table SI of the Supplementary Material. A reproducible clean alloy surface was achieved by polishing with abrasive paper (P240,  $\text{Al}_2\text{O}_3$  grains, Mirka). To study the scalability of the technology for preparation of nanostructured coatings for industrial applications on arbitrarily shaped high-precision components, Al alloy substrates were prepared for satellites ESTCube-2 and WISA Woodsat. On the former satellite, a cover panel was prepared by machine milling from an Al–Mg alloy sheet containing 2.9% Mg. The components for WISA Woodsat were 3D printed with an industrial metal 3D printer EOS M290 (EOS GmbH) from Al alloy powder, EOS Aluminum AlSi10Mg (EOS GmbH). Prior to coating, all loose particles and organic contamination were removed via a standard pre-treatment, by first rinsing with deionized water

and then by three solvents in an ultrasonic bath: 3 min in toluene (purity 99.5%, Reahim), 3 min in acetone (purity 99.5%, Sigma-Aldrich), and finally 3 min in isopropanol (purity 99.5%, Sigma-Aldrich). The 3D printed substrates received an additional chemical treatment for removing impurities and near-surface metal oxides, which consisted of a) immersion in 10% NaOH solution (purity  $\geq 98\%$ , Sigma-Aldrich) for 1 min, b) rinsing with deionized water, c) immersion in concentrated  $\text{HNO}_3$  (purity 65%, Sigma-Aldrich) for 1 min, and d) rinsing with deionized water. The latter treatment was necessary because mechanical polishing could not be used for the high-precision components.

**Anodizing of the substrates.**—The anodizing process was carried out in a two-electrode setup with a PS 8360-10 DT 1 kW power supply (Elektro-Automatck GmbH), using a stainless-steel bath as the cathode and the Al alloy substrates as the anode. A 15% sulfuric acid solution was used as the anodizing electrolyte, and its temperature was maintained at  $1 \text{ }^\circ\text{C} \pm 0.5 \text{ }^\circ\text{C}$  by surrounding the stainless-steel anodizing bath with an additional ice bath. A 15% sulfuric acid solution was prepared from concentrated sulfuric acid (SA; 95%–97%, Honeywell, Fluka). For the potentiostatic anodizing process, the voltage was set at 10 V for thinner and 20 V for thicker AAO, and the maximum current density at the beginning of both processes was set at  $12.5 \text{ mA cm}^{-2}$ .

**Sealing and coating of anodized substrates by ALD.**—ALD was used to seal and coat the nano-scaled pores of anodic aluminum oxide with different metal oxides, such as  $\text{TiO}_2$ ,  $\text{Al}_2\text{O}_3$ , an  $\text{Al}_2\text{O}_3$ - $\text{TiO}_2$  mixture, or an  $\text{Al}_2\text{O}_3/\text{TiO}_2$  nanolaminate. Ceramic films with target thicknesses of 50 and 110 nm were deposited on the smaller substrates in a low-pressure flow-type reactor<sup>29</sup> at  $125 \text{ }^\circ\text{C}$  by using  $\text{TiCl}_4$  (Aldrich, purity 99.9%) and  $\text{Al}(\text{CH}_3)_3$  (purity 98%, Strem Chemicals) as metal precursors and water as the source of oxygen. Larger substrates were coated using the same precursors and deposition temperatures in a commercial Picosun® R200 (Picosun OY) ALD reactor.<sup>27</sup> In the nanolaminate, the bottom layer consisted of 20 nm  $\text{Al}_2\text{O}_3$ , followed by 10 nm  $\text{TiO}_2$  and 10 nm  $\text{Al}_2\text{O}_3$  layers in turn until the total target thickness of 50 or 110 nm was reached, with  $\text{TiO}_2$  always as the top layer. The substrates, which were sealed by ALD with a 50 nm material, were used for thorough studies. For the salt-spray test, the thickness of the sealing material was increased to 110 nm. A 50 nm thick  $\text{Al}_2\text{O}_3$ - $\text{TiO}_2$  mixture layer was grown with 250 ALD supercycles as described earlier.<sup>28</sup> Each successive supercycle consisted of one full ALD cycle for the deposition of an  $\text{Al}_2\text{O}_3$  sublayer and two full ALD cycles for the deposition of a  $\text{TiO}_2$  sublayer, thus the mixture was built by successive one alumina sublayer following two titania sublayers. This was performed to compensate for two times lower growth rate of titania per full growth cycle in comparison with the growth rate of alumina.<sup>30</sup> As shown in our earlier work the mixture layer deposited by exact the same conditions onto Si substrate has thickness of 52 nm, determined via X-ray reflection, and has following composition: Ti = 33.3, Al = 25.3, O = 40.0, and residual Cl = 1.4 mass%, determined via thin film X-ray fluorescence analysis.<sup>28</sup> Based on the analysis data the  $\text{Al}_2\text{O}_3$ - $\text{TiO}_2$  mixture has the oxides ratio of 1:1.5.

**Surface and coating characterization.**—HR-SEM and local analyses were performed using a Helios NanoLab 600 (FEI) equipped with an energy-dispersive X-ray spectrometry (EDX) analyzer INCA Energy 350 (Oxford Instruments) and focused ion beam (FIB) device. HR-SEM surface and cross-sectional studies were performed using a 10 kV accelerating voltage for the primary electrons. For the SEM-EDX studies, an accelerating voltage of 5–30 kV was used. The cross-sections and (S)TEM lamellae were prepared as follows. Prior to cross-sectioning, the surface of the sample was locally coated with a  $\sim 1 \mu\text{m}$  thick protective Pt layer using first a 10 kV electron beam and then a 30 kV focused Ga ion beam. Both beams scanned a predetermined area and decomposed an organometallic platinum compound, which was sprayed onto the

surface with a needle. Subsequently, FIB milling was performed through the Pt-layer using a high voltage (30 kV) and an intense (21 nA) focused ion beam directed at the surface at 90 degree angle. The final cleaning of the cross sections was carried out at the same acceleration voltage using a beam current of 9 nA. The milling and cleaning processes were monitored using ion beam generated secondary electrons. The (S)TEM lamellae were cut out using an accelerating voltage of 30 kV and a beam current of 9 nA. The lamellae were thinned to electron transparency using the same accelerating voltage, gradually reducing the beam current and periodically checking the transparency of the lamellae with the

electron beam and a STEM retractable detector. The lamellae were then polished by gradually reducing the acceleration voltage and the beam current in order to avoid amorphization of the lamellae surface layers caused by the ion beam. The final polishing was done with 2 kV and 3 pA ion beam. The HR-STEM and -EDX studies were performed with a Titan 200 (FEI) analytical probe-corrected high-resolution electron microscope, equipped with a ChemiSTEM 4 SuperX SDD EDX system (FEI/Bruker), using primary electrons with acceleration voltage of 200 kV. The hardness of the coatings was measured with a Nano Indenter G200 (Agilent Technologies) in the continuous stiffness measurement (CSM) mode. The plots were

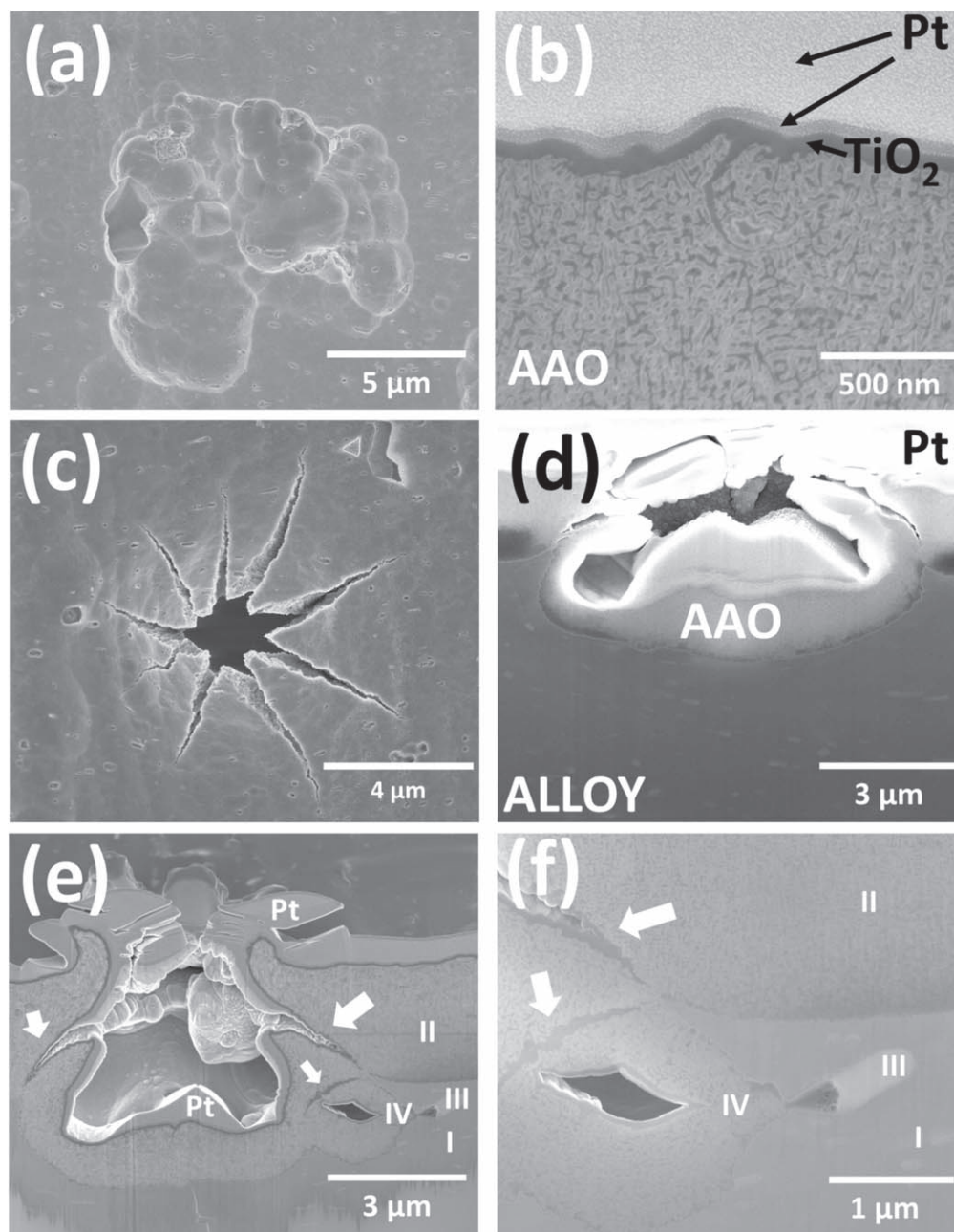


**Figure 1.** SEM images of the AAO layer obtained by potentiostatic anodizing at 20 V, 1 °C depicting the most abundant shallow craters from the removal of micrometric IMP-s (a), a FIB made cross-section of a sealed AAO with ALD TiO<sub>2</sub> layer, which visualize well the 3D structure of branched nanopores (b), top view of a cracked crater (c), FIB-made cross-section of a cracked crater (d); a cross-section of another cracked crater sealed with TiO<sub>2</sub> using ALD to demonstrate the efficiency of sealing (e); image (f) to show the right part of image (e) at higher magnification. In images (e) and (f), the regions of metal substrate, sealed nanoporous AAO layer and partially removed IMP are labelled I, II and III, respectively. Arrows indicate cracks, and label IV indicates the gap left by the IMP during the anodizing process and subsequently closed by ALD.

obtained by averaging the results of 20 nanoindentation tests for each sample. Hardness and Young's modulus values were determined at their maximum values in the corresponding plots.

**Testing of the coatings.**—The corrosion resistance of coated and uncoated Al alloy substrates was studied by linear sweep voltammetry (LSV) and electrochemical impedance spectroscopy (EIS), and tested via immersion in an unmixed salt solution, neutral salt spray, and flux of atomic oxygen. The immersion tests were carried out in a naturally aerated neutral (pH  $\sim$  6.5) 0.5 M NaCl (purity  $\geq$ 99.8%, Sigma-Aldrich) solution at room temperature ( $22 \text{ }^\circ\text{C} \pm 2 \text{ }^\circ\text{C}$ ), using smaller and larger Al-alloy substrates. Preliminary tests with smaller plates took place for up to 1 year, and tests with larger plates took place for up to 1000 h. Salt spray tests for up to 1000 h also took place and were performed in a ClimaCORR<sup>®</sup> 400-FL chamber (VLM GmbH) at  $35 \text{ }^\circ\text{C} \pm 2 \text{ }^\circ\text{C}$  using a 5% NaCl (SaliCORR) solution at pH 6.5–7.0, according to ISO 9227:2012. The samples were photographed before, periodically during, and after the immersion and salt-spray tests. Electrochemical corrosion studies were carried out in a PTC1<sup>™</sup> Paint Test Cell (Gamry) using a potentiostat Reference 600 (Gamry), a saturated calomel reference electrode (SCE), and a Pt wire as the counter electrode. The electrolyte used in the electrochemical tests was a naturally aerated 0.5 M NaCl ( $\geq$ 99.8%, Sigma-Aldrich) solution, and the experiments were performed at room temperature,  $23 \text{ }^\circ\text{C} \pm 1 \text{ }^\circ\text{C}$ . A reproducible surface area of  $1 \text{ cm}^2$  was achieved on the coated and uncoated smaller substrates using  $1 \text{ cm}^2$  electrochemical sample masks (PortHoles<sup>™</sup>, Gamry). For LSV testing at a scan rate of  $1 \text{ mV s}^{-1}$ , the initial and end potentials were  $-1 \text{ V}$  and  $+1 \text{ V}$  vs SCE, respectively. All potentials in this work were compared with SCE, unless otherwise mentioned. The current density ( $j_{1V}$ ) was measured at  $1 \text{ V}$  to evaluate the performance of the coatings at anodic potentials. The EIS measurements were performed twice during 24 h immersion in 0.5 M NaCl at open circuit potential (OCP). The first measurement was carried out at the start of immersion after the sample had stabilized for 30 min, and the second measurement after 24 h of immersion. The measurements were performed in the frequency range  $10^{-2}$ – $10^6 \text{ Hz}$ , with an AC perturbation amplitude of  $10 \text{ mV}$  (RMS). Echem Analyst<sup>™</sup> (Gamry) software was used to interpret the EIS data using equivalent circuit models.

To evaluate the performance of the nanostructured coating in space, the coated substrate was tested by exposure to a flux of atomic oxygen (ATOX test) at a low earth orbit simulation facility (LEOX).<sup>31</sup> In the test, the atomic oxygen flow was  $2.7 \times 10^{21} \text{ atoms cm}^{-2}$ , which is comparable to 1.1 years of exposure to a direct flux

of atomic oxygen in low Earth orbit at an altitude of 400 km, the same as for the International Space Station.

## Results

Studies of anodized substrates (see also Supplementary Material) have shown that in order to achieve complete protection against corrosion, it is necessary to seal all the nano-scaled pores in the AAO layer as well as the cracks in it, and any leftover intermetallic particle (IMP) left inside particle craters. For this purpose, ALD was used to deposit 50–110 nm of  $\text{Al}_2\text{O}_3$ ,  $\text{TiO}_2$ ,  $\text{Al}_2\text{O}_3$ - $\text{TiO}_2$  mixture, or  $\text{Al}_2\text{O}_3/\text{TiO}_2$  nanolaminate coatings on anodized substrates using appropriately chosen ALD parameters.<sup>27</sup> The temperature window for coating AA2024-T3 alloy is actually quite narrow. The alloy is artificially aged at  $180 \text{ }^\circ\text{C}$  in the thermal treatment process. Therefore,  $125 \text{ }^\circ\text{C}$  is a temperature at which the alloy can be processed for several hours without changing its mechanical properties. On the other hand, alumina and titania grown at this temperature by thermal ALD are amorphous.<sup>26,27</sup> Amorphous phase is preferred for corrosion protection coating because the material does not contain crystalline grains and defective interfaces between them that allow fast diffusion of corrosive species through the coating.

**The effect of potentiostatic anodizing on the Al-alloy.**—The pretreatment of the Al alloy was performed by potentiostatic anodization at  $20 \text{ V}$ ,  $1 \text{ }^\circ\text{C}$  because it can be easily performed with a low-cost anodizing setup while also having a good control over the temperature of the electrolyte by using an external ice bath. Anodizing at temperatures lower than room temperature would also result in denser and harder AAO, which is desired in practical applications.<sup>19,20</sup>

High-resolution scanning electron microscopy (HR-SEM) images of the AAO shown in Fig. 1a reveal shallow craters that were likely left behind by the removal of the most abundant  $\text{Al}_2\text{CuMg}$  IMPs. Similar craters are seen by the use of potentiodynamic anodizing in our previous paper.<sup>27</sup> Furthermore, the focused ion beam made cross section depicted in Fig. 1b shows that the AAO obtained with potentiostatic anodizing is denser than that obtained with potentiodynamic anodizing, see latter in Fig. 7e, in the earlier paper.<sup>27</sup> However, current study also revealed a new type of cracked crater in AAO (Fig. 1c), which was not observed in the potentiodynamic anodizing process. There were only a few such cracked craters, but surface studies suggest that it is a recurring phenomenon. Surprisingly, the edges of the cracked craters protrude outwards. We believe that such features could have been created by the removal of partially exposed IMPs that were deeper in the alloy.

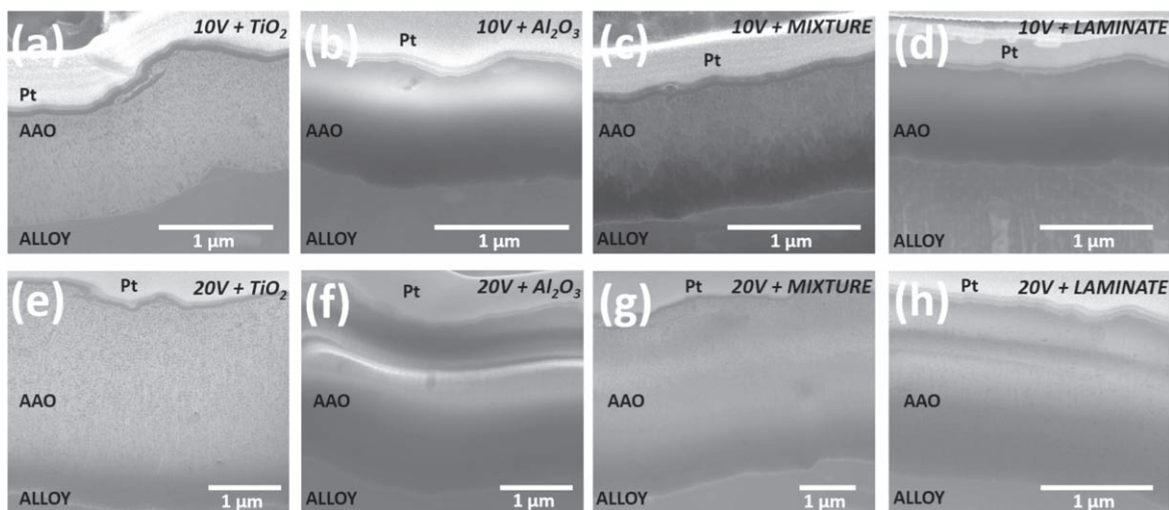


**Figure 2.** SEM images of the FIB made cross-sections of Al-alloy substrates anodized at  $10 \text{ V}$ ,  $1 \text{ }^\circ\text{C}$  (a)–(d) and  $20 \text{ V}$ ,  $1 \text{ }^\circ\text{C}$  (e)–(h), having the AAO layer sealed by ALD with  $50 \text{ nm}$   $\text{TiO}_2$  (a), (e),  $\text{Al}_2\text{O}_3$  (b), (f),  $\text{Al}_2\text{O}_3$ - $\text{TiO}_2$  mixture (c), (g) or  $\text{Al}_2\text{O}_3/\text{TiO}_2$  nanolaminate (d), (h).

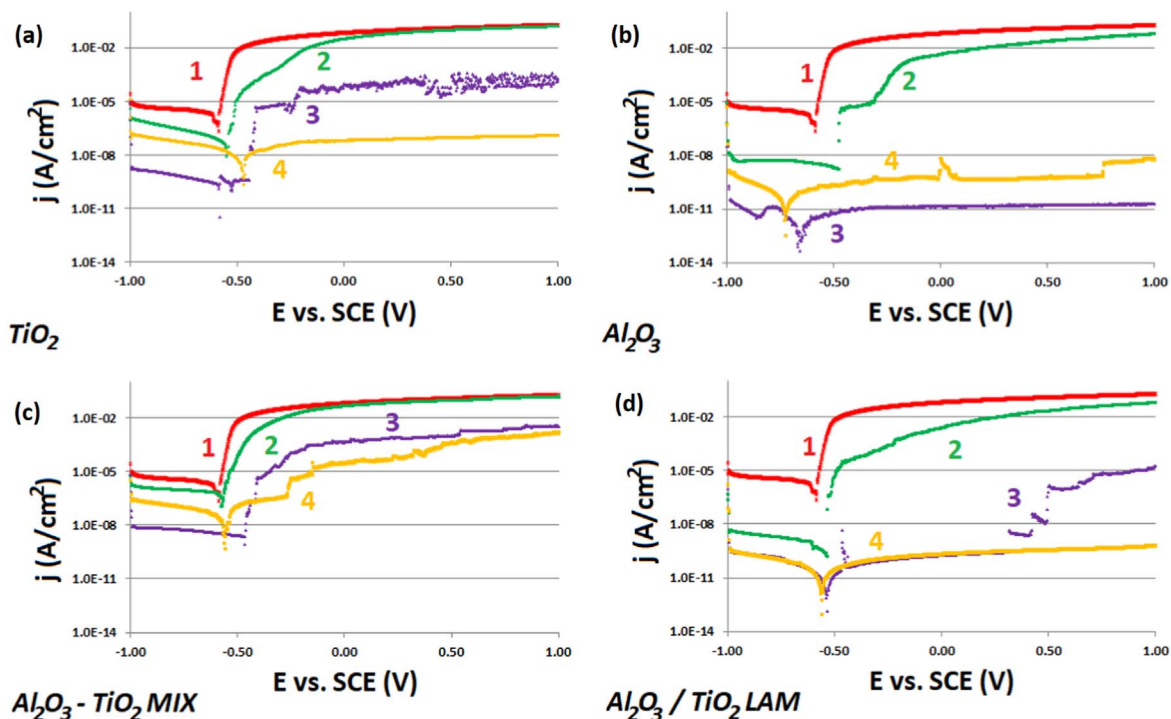


**Figure 3.** The results of LSV corrosion tests performed in naturally aerated 0.5 M NaCl solution for the Al-alloy substrates that were coated using ALD with 50 nm TiO<sub>2</sub> (a), Al<sub>2</sub>O<sub>3</sub> (b), Al<sub>2</sub>O<sub>3</sub>-TiO<sub>2</sub> mixture (c) or Al<sub>2</sub>O<sub>3</sub>/TiO<sub>2</sub> nanolaminate (d), showing the polarization curves for the: polished sample (1), polished samples coated by ALD (2), samples that were anodized at 10 V, 1 °C, and coated by ALD (3), samples that were anodized at 20 V, 1 °C, and coated by ALD (4).

The rapid removal of IMPs during the initial stages of anodizing would take place through the narrow path on the top, which could become clogged and result in a buildup of pressure and eventually rupture. Further cracking would also be promoted by the mechanical stresses created by the expansion of the material during anodization, as aluminum oxide takes up more space than the original metal. It is also important to mention that the cracks penetrate deeply into the AAO layer and may even reach the metal (Fig. 1d). This would be problematic in practical applications because such cracks would also provide a pathway for corrosive species to the metal substrate. To confirm the presence of such dangerous pathways, we used electroplating to visualize the defects, as in a previous work.<sup>32</sup> Study of the AAO layer with Ag electrodeposition is discussed in the Supplementary Material in detail. Figures 1e and 1f show a cross-section of another cracked crater coated with ALD deposited TiO<sub>2</sub> nanolayer, see the darker stripe around the crater and cracks. The images demonstrate the conformal coating of the crater wall and successful sealing of tip part of the cracks (marked with arrows), and the nanochannel connecting the partially removed IMP with the crater (IV). Thus, all potentially corrodible areas are well sealed. At the bottom of the crater, in the center, it is seen a mound formed by Pt that moved through the crater opening during the deposition of the Pt-layer by FIB. For this reason, the TiO<sub>2</sub> ALD coating is under the Pt mound.

**Thorough study of the AAO layer sealing with varied ALD top coatings.**—The purpose of this thorough study was to determine the best possible material for sealing the AAO layer obtained by potentiostatic anodizing to create an efficient nanostructured coating. For this purpose, ALD was used to grow Al<sub>2</sub>O<sub>3</sub>, TiO<sub>2</sub>, an Al<sub>2</sub>O<sub>3</sub>-TiO<sub>2</sub> mixture, or Al<sub>2</sub>O<sub>3</sub>/TiO<sub>2</sub> nanolaminate films on anodized substrates using appropriately chosen ALD pulse times.<sup>27</sup> In these studies, a target thickness of 50 nm was deemed to be sufficient in the ALD process to seal the nanoscale pores, as observed in Fig. 1b.

**SEM-FIB studies of nanostructured coatings.**—SEM-FIB studies revealed that the total thickness of the coatings was within the

targeted  $\leq 5 \mu\text{m}$  range (Fig. 2). As expected, the thickness of the coating was mainly determined by the potential used in the anodization process. In particular, anodizing at 10 V, 1 °C resulted in a coating thickness of  $\sim 1 \mu\text{m}$  (Figs. 2a–2d). In comparison, anodizing at 20 V, 1 °C provided coatings that had a thickness of 2–4  $\mu\text{m}$  (Figs. 2e–2h). In addition, the pore diameter and overall volume in a unit are larger in the latter case, as can be seen by comparing the cross-sectional images sealed by TiO<sub>2</sub> AAO in Figs. 2a and 2e (note that image a has  $1.5 \times$  higher magnification than image e). The SEM-FIB studies show that by using appropriately chosen ALD pulse times, it is possible to efficiently seal the nanoscale pores in the AAO layer with various ceramic materials such as TiO<sub>2</sub> (Figs. 2a, 2e), Al<sub>2</sub>O<sub>3</sub> (Figs. 2b, 2f), Al<sub>2</sub>O<sub>3</sub>-TiO<sub>2</sub> mixture (Figs. 2c, 2g), and Al<sub>2</sub>O<sub>3</sub>/TiO<sub>2</sub> nanolaminate (Figs. 2d, 2h). It should be noted that the first layer of the nanolaminate consists of 20 nm of Al<sub>2</sub>O<sub>3</sub>, which seals most of the nanoscale pores in the AAO layer. Consequently, in the case of the nanolaminate, the amount of TiO<sub>2</sub> in the sealed AAO layer is small, as it can only be deposited into wider pores, cracks, and craters that are not completely sealed by the first 20 nm of Al<sub>2</sub>O<sub>3</sub>. The sealing of nanoscale pores also has an impact on the overall conductivity of the entire nanostructured coating. For instance, sealing with TiO<sub>2</sub> results in a more conductive coating, which makes it easier to study via HR-SEM as it does not suffer from extensive charging, which has a negative impact on the imaging process for visualization of the internal nanoscale structure (Fig. 2a). In contrast, sealing the AAO with Al<sub>2</sub>O<sub>3</sub> (Fig. 2b) or Al<sub>2</sub>O<sub>3</sub>/TiO<sub>2</sub> nanolaminate (Fig. 2d) results in a more dielectric coating, which is observed in the SEM studies. However, the top TiO<sub>2</sub> layer in the nanolaminate provides near-surface conductivity owing to its semiconducting properties (Fig. 2d). Using the Al<sub>2</sub>O<sub>3</sub>-TiO<sub>2</sub> mixture to seal the AAO (Fig. 2c) results in a coating that has better overall conductivity than that obtained by sealing with Al<sub>2</sub>O<sub>3</sub> (Fig. 2b). Based on these observations, it is clear that the electrical conductivity of nanostructured coatings can be designed to satisfy the requirements of specific applications. Dielectric coatings can be made by sealing and coating AAO with Al<sub>2</sub>O<sub>3</sub> whereas semiconductor coatings can be made by sealing and coating AAO

**Table I. Data obtained via LSV and nanoindentation studies on bare and coated substrates with different pre-treatments and 50 nm ceramic films grown by ALD.**

Substrate pre-treatment	ALD coating	Pitting potential $E_{\text{pit}}$ , V	Current density $j_{1V}$ , A cm <sup>-2</sup>	Coating efficiency, CE (Eq. 1)	$H_{\text{max}}$ , GPa	$E_{\text{max}}$ , GPa
Standard	—	-0.59	0.20 <sup>a)</sup>	—	3.0 ± 1.2	100 ± 13
Standard	TiO <sub>2</sub>	-0.53	0.16	0.20	3.3 ± 0.9	96 ± 23
Standard	Al <sub>2</sub> O <sub>3</sub>	-0.48	6.2 × 10 <sup>-2</sup>	0.68	4.1 ± 1.3	93. ± 23
Standard	Mixture <sup>b)</sup>	-0.57	0.16	0.20	3.3 ± 1.4	98 ± 34
Standard	Laminate <sup>c)</sup>	-0.54	6.4 × 10 <sup>-2</sup>	0.68	3.5 ± 0.8	96 ± 10
10 V anod.	—	-0.56	0.13	0.33	3.0 ± 1.3	88 ± 22
10 V anod.	TiO <sub>2</sub>	-0.45	1.5 × 10 <sup>-4</sup>	1.00	5.5 ± 1.8	102 ± 18
10 V anod.	Al <sub>2</sub> O <sub>3</sub>	N/A	1.8 × 10 <sup>-11</sup>	1.00	7.2 ± 1.8	121 ± 26
10 V anod.	Mixture	-0.46	3.5 × 10 <sup>-3</sup>	0.98	5.2 ± 2.2	100 ± 37
10 V anod.	Laminate	0.35	1.7 × 10 <sup>-5</sup>	1.00	6.5 ± 1.3	111 ± 17
20 V anod.	—	-0.52	0.14	0.30	2.3 ± 0.5	75 ± 11
20 V anod.	TiO <sub>2</sub>	N/A	1.3 × 10 <sup>-7</sup>	1.00	4.5 ± 1.2	95 ± 20
20 V anod.	Al <sub>2</sub> O <sub>3</sub>	0.75	6.6 × 10 <sup>-9</sup>	1.00	5.2 ± 1.6	95 ± 25
20 V anod.	Mixture	-0.27	1.6 × 10 <sup>-3</sup>	0.99	3.0 ± 0.9	70 ± 8
20 V anod.	Laminate	N/A	6.5 × 10 <sup>-10</sup>	1.00	5.5 ± 1.3	99 ± 19

a)  $j_{\text{max}} = 20\text{nA}$ . b) - Al<sub>2</sub>O<sub>3</sub>-TiO<sub>2</sub>. c) - Al<sub>2</sub>O<sub>3</sub>/TiO<sub>2</sub>.

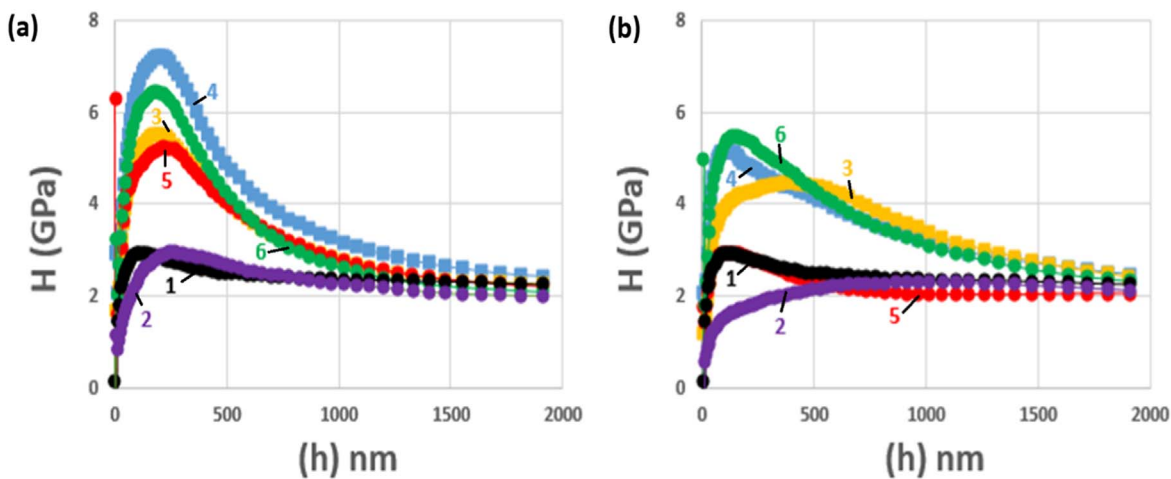


**Figure 4.** Surface hardness,  $H$ , vs indentation depth,  $h$ , curves of anodized at 10 V, 1 °C (a) and 20 V, 1 °C (b) samples. The curves 1 belonging to just-polished substrate and curves 2 to anodized samples, other curves to anodized and ALD sealed and coated samples, using 50 nm of TiO<sub>2</sub> (curve 3), Al<sub>2</sub>O<sub>3</sub> (curve 4), Al<sub>2</sub>O<sub>3</sub>-TiO<sub>2</sub> mixture (curve 5) or Al<sub>2</sub>O<sub>3</sub>/TiO<sub>2</sub> nanolaminate (curve 6).

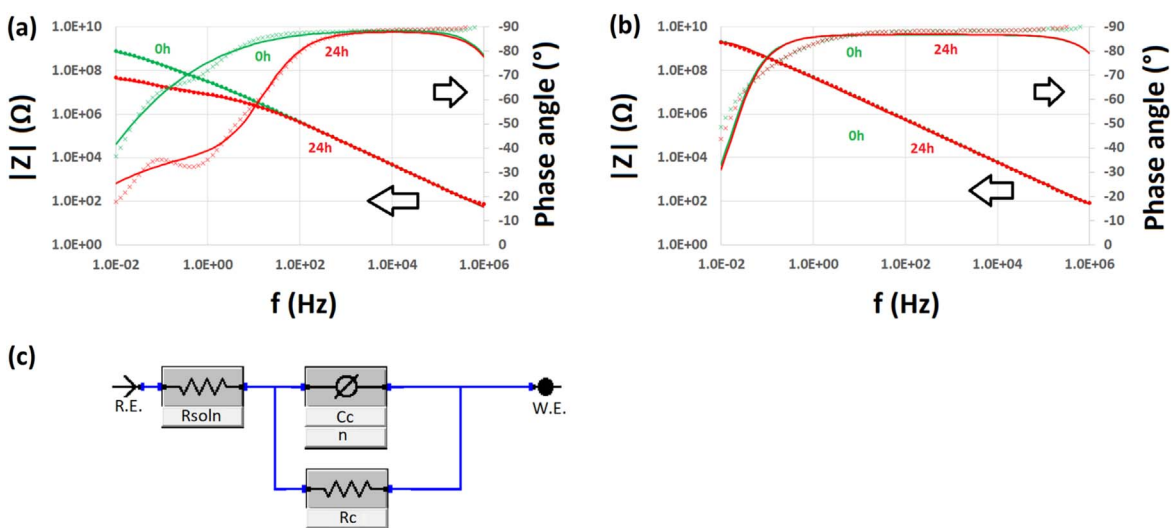


**Figure 5.** EIS study results: Bode plots for the substrates with nanostructured coatings prepared by anodizing at 20 V, 1 °C and sealed by ALD with 50 nm (a) and 110 nm nanolaminate (b). In Bode plots the markers show experimental and linear modelled values. An equivalent circuit model (ECM) given in (c) was used for modelling the plot curves in (b).

with TiO<sub>2</sub>. Alternatively, a coating can be made dielectric in the depth direction by sealing the AAO with Al<sub>2</sub>O<sub>3</sub> or semiconducting on the top surface by applying a top layer that includes TiO<sub>2</sub>.

*Linear sweep voltammetry study of nanostructured coatings.*—Corrosion testing by linear sweep voltammetry was carried out on polished and anodized substrates sealed and coated by ALD with

50 nm films (Fig. 3, Table I). In comparison with the bare polished sample, all the coated substrates exhibited lower current values across the entire scan range, which indicates an improvement in corrosion resistance. However, a more detailed comparison can be made by observing the pitting potential ( $E_{cor}$ ) and current density ( $j_{1V}$ ) values at 1 V. The latter can also be used to calculate the short-term coating efficiency ( $CE$ ), similarly to our previous study:<sup>28</sup>

**Table II.** Calculated ECM (Fig. 5c) variables for Al alloy substrates with nanostructured coating prepared in this paper (Fig. 5b) and in Ref. 27 before and after 24 h immersion in salt solution.

EMC variables	Coatings			
	Anodized at 20 V, 1 °C plus 110 nm nanolaminate		Anodized at 10 V, 22 °C plus 100 nm laminate <sup>27</sup>	
Immersion time, h	0.5	24	0.5	24
Fixed $R_{soln}$ , $\Omega \text{ cm}^2$	10.0	10.0	10.0	10.0
$R_c$ , $\Omega \text{ cm}^2$	$2.6 \times 10^9$	$2.4 \times 10^9$	$1.2 \times 10^9$	$1.3 \times 10^9$
$C_c$ , $\text{F cm}^{-2} \text{ s}^{n-1}$	$3.7 \times 10^{-9}$	$3.7 \times 10^{-9}$	$7.2 \times 10^{-9}$	$7.2 \times 10^{-9}$
$n$	0.96	0.96	0.97 <sup>a)</sup>	0.97 <sup>a)</sup>

a)  $n = n_2$ .



$$CE = 1 - (j_{1V}/j_{max}). \quad [1]$$

According to the measured polarization curves depicted in Fig. 3 and summarized data given in Table I, no pitting corrosion was observed for the substrates that were, first, anodized at 20 V, 1 °C and sealed with TiO<sub>2</sub> (Fig. 3a, curve 4), second, anodized at 10 V, 1 °C and sealed with Al<sub>2</sub>O<sub>3</sub> (Fig. 3b, curve 3), and third, anodized at 20 V, 1 °C and sealed with Al<sub>2</sub>O<sub>3</sub>/TiO<sub>2</sub> nanolaminate (Fig. 3d, curve 4). These results indicate that these coatings were defect-free and that the corrosive species could not come into direct contact with the metal substrate. In the case of sealing the AAO with TiO<sub>2</sub>, the measured current densities across the entire scan range were notably higher than those of the samples where the AAO was sealed by Al<sub>2</sub>O<sub>3</sub> or by Al<sub>2</sub>O<sub>3</sub>/TiO<sub>2</sub> nanolaminate. This can be explained by the higher conductivity of amorphous TiO<sub>2</sub> in comparison with Al<sub>2</sub>O<sub>3</sub>, which was also utilized in our first study to visualize the pores in the AAO layer.<sup>27</sup> Photographs of the substrates after the LSV tests (Fig. S5 (available online at [stacks.iop.org/JES/169/071503/mmedia](https://stacks.iop.org/JES/169/071503/mmedia)) in the Supplementary Material) are in good agreement with the measured polarization curves depicted in Fig. 3.

**Hardness of nanostructured coatings.**—Nanoindentation studies showed that the measured hardness (*H*) and Young's modulus (*E*) values depend on the surface pre-treatment, as well as on the material grown by ALD (Fig. 4 and Table I).

The coatings grown by ALD directly onto the substrate slightly increased the surface hardness value in comparison with the bare substrate (Table I). However, the differences observed in the

measurements were negligible, except for the alumina film, which was somewhat harder than the substrate. It should be noted that the hardness of the coatings grown by ALD was studied separately in our previous study, where the materials were grown on Si substrates.<sup>28</sup> Comparing the hardness values of the same coatings deposited on a relatively soft Al alloy (*H* = 3 GPa; Table I) and on a hard Si substrate (*H* = 13 GPa),<sup>28</sup> the former values are considerably lower than the latter. It seems that during the nanoindentation of thin coatings on a soft substrate, the ceramic coating is cracked and penetrated by the tip at the very beginning of the indentation. Therefore, the deformed substrate has a greater impact on the measured *H* values than the coatings do. However, the situation is different for substrates with thicker non-sealed AAO layers. For instance, the ~1 μm thick AAO obtained by anodizing 10 V, 1 °C exhibited a hardness similar to that measured for the substrate. However, the *H*-curve in Fig. 4a (curve 2) shows that the non-elastic deformation starts at the very beginning of the indentation process. This is much more obvious for the AAO obtained at 20 V, 1 °C, which had a thickness of ~2 μm (Fig. 4b, curve 2). This behavior can be explained by the structure of AAO, in which the pores have a nanometric diameter and the separating ceramic walls have a similar thickness. It is also noted that thicker AAO exhibited lower hardness values than those of thinner AAO. As shown in Figs. 2a and 2e, the thicker AAO has a somewhat lower density owing to wider pores and larger volume in a unit, which explains its lower hardness in both the non-sealed and sealed coatings (Fig. 4 and Table I).

Sealing AAO by ALD with different materials resulted in nanostructured coatings that were mostly harder than the Al alloy (Fig. 4 and Table I). This can be explained by filling of empty pores

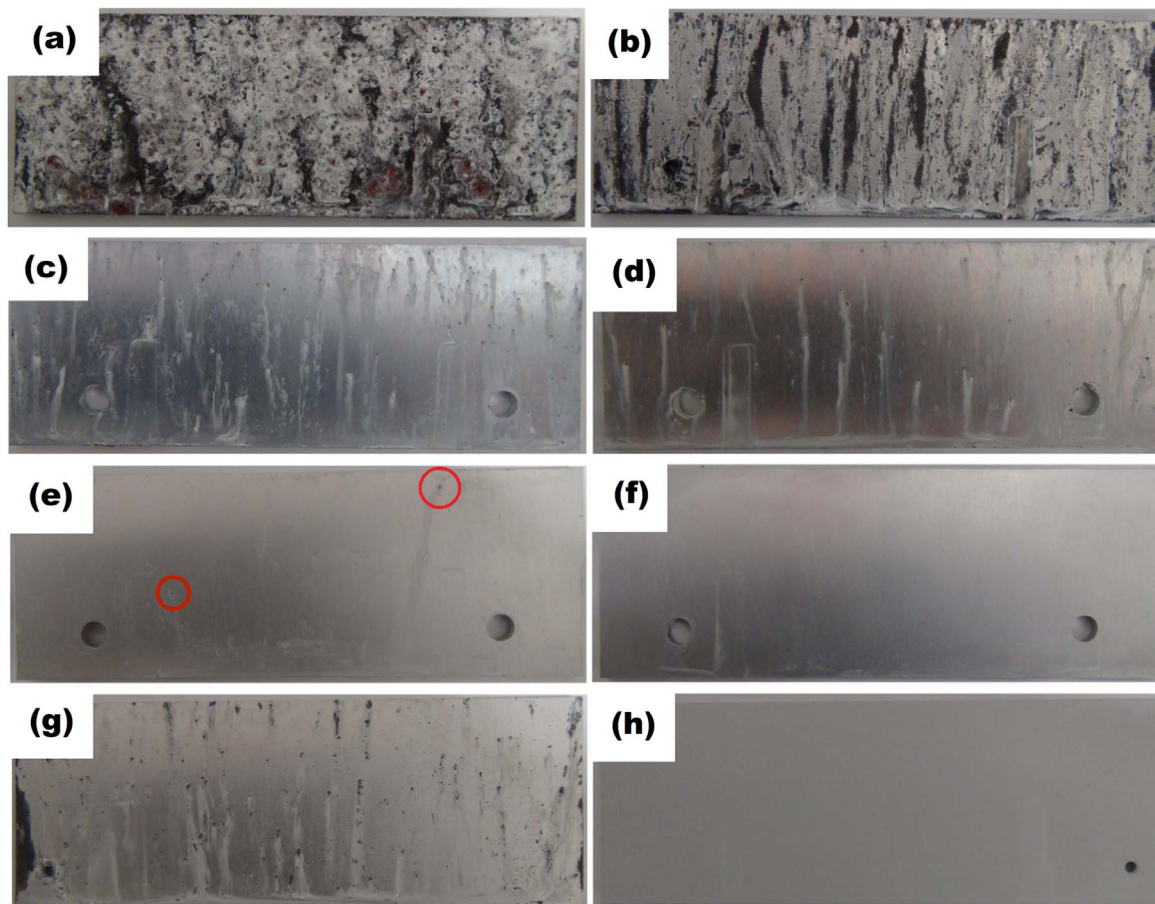


**Figure 6.** Photos of 40 × 110 mm<sup>2</sup> AA2024-T3 samples after 1000 h ISO 9227 salt spray test at 35 °C depicting a just-polished sample (a), sample just-anodized at 20 V, 1 °C (b), sample with deposits onto the polished substrate of 50 nm nanolaminate (c) and 110 nm nanolaminate (d), sample anodized at 20 V, 1 °C and sealed with 50 nm nanolaminate (e) and 110 nm nanolaminate (f), sample anodized at 20 V, 1 °C following hydrothermal sealing (g), sample anodized at 20 V, 23 °C and sealed with Rust Stop paint (h).

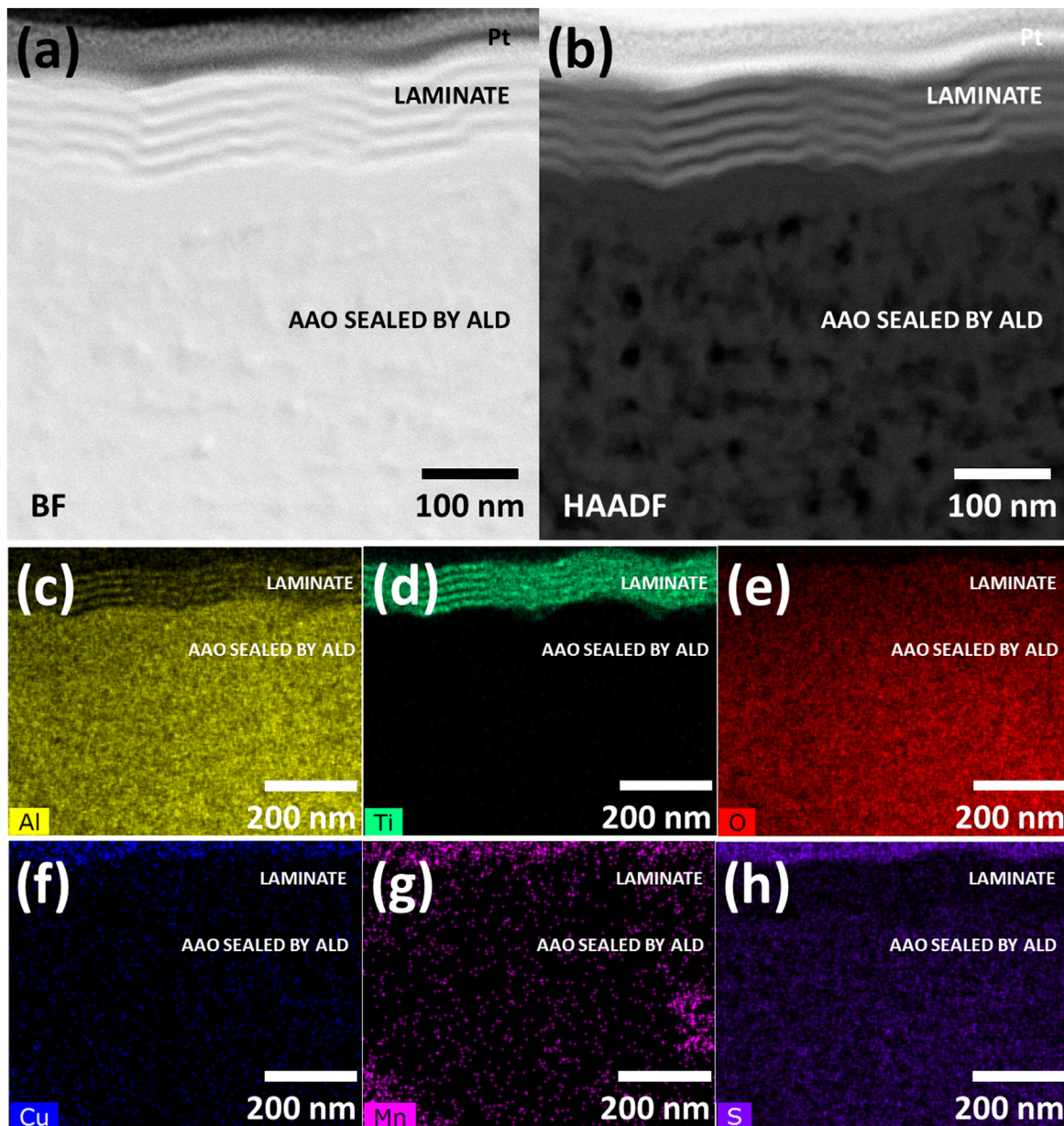


**Figure 7.** STEM study results of nanostructured coating, depicting a) bright field and b) high-angle annular dark field (HAADF) images made of a lamella prepared from the coating by FIB. STEM-EDX analysis results of the same lamella show the distribution of Al (c), Ti (d), O (e), Cu (f), Mn (g), and S (h) in the top part of the nanostructured coating.

in the hard AAO layer with ceramic material, which increases the overall density of the coating. Furthermore, the materials used for sealing also have distinct hardness, which contributes to the mechanical properties of the nanostructured coating. The hardest coatings were obtained using  $\text{Al}_2\text{O}_3$  or  $\text{Al}_2\text{O}_3/\text{TiO}_2$  nanolaminate to seal the AAO (Fig. 4, curves 4, 6 and Table I). This is not surprising, as  $\text{Al}_2\text{O}_3$  and  $\text{Al}_2\text{O}_3/\text{TiO}_2$  nanolaminate films grown by ALD on Si substrates also exhibit the highest hardness values.<sup>28</sup>

Furthermore, the denser AAO obtained by anodizing at 10 V, 1 °C also provided harder nanostructured coatings than using 20 V, 1 °C anodizing for pre-treatment (Fig. 4, curves 3–6 and Table I). The lowest hardness was observed for the nanostructured coating, which was prepared by anodizing at 20 V, 1 °C and sealed with the  $\text{Al}_2\text{O}_3$ - $\text{TiO}_2$  mixture (Fig. 4b, curve 5, and Table I).

**Characterization and testing of best-performing nanostructured coating.**—The studies described above showed that only three

recipes resulted in a nanostructured coating that did not exhibit pitting corrosion in the linear sweep voltammetry (LSV) tests and that using 20 V for anodizing generally results in better short-term corrosion protection coatings (Fig. 3). On the other hand, we have to consider the fact that aluminum oxide is converted into aluminum hydroxide by staying in a moist environment or aqueous media for a long time.<sup>28</sup> Therefore, pure alumina coatings are impractical. Furthermore, from these three coatings, the highest surface hardness was observed for the substrate that was anodized at 20 V, 1 °C and then sealed by ALD with 50 nm nanolaminate (Fig. 4). Based on these results, we further studied and optimized the best-performing coating recipe.

**EIS study of nanostructured coating.**—The purpose of the electrochemical impedance spectrometry study depicted in Fig. 5 was to evaluate the stability of the best-performing nanostructured coating before and after 24 h immersion in a neutral 0.5 M NaCl

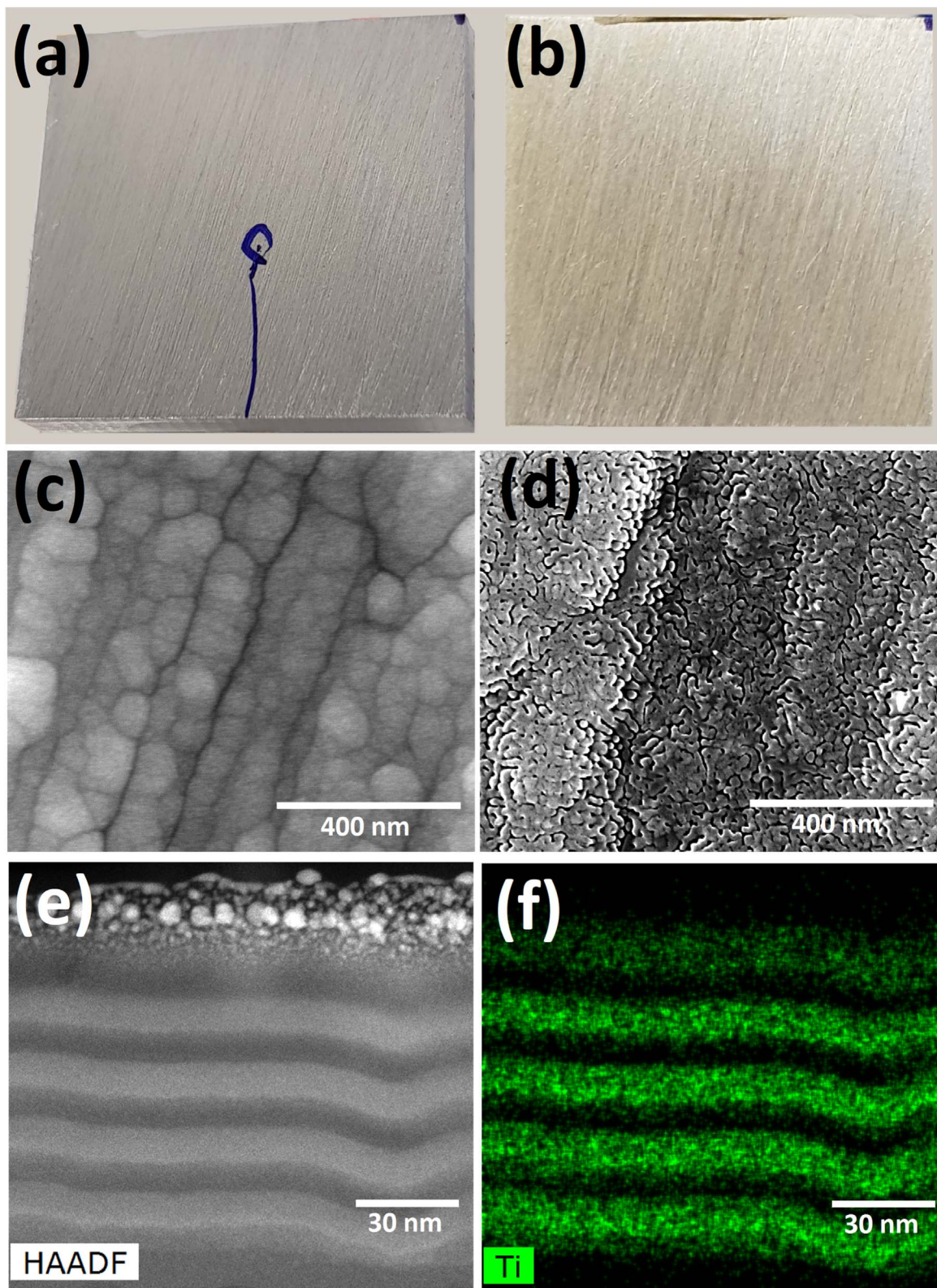


**Figure 8.** Photos, SEM and STEM images of an as-prepared and ATOX-tested nanostructured coating, made by anodizing at 20 V, 1 °C following enhancement by ALD by adding a 110 nm thick nanolaminate: a) photo of the substrate before ATOX test and b) after ATOX test, c) HR-SEM image of the nanostructured coating before ATOX test and d) after ATOX test, e) STEM high-angle annular dark field image of the lamella of the nanostructured coating after ATOX test and f) with overlay of the Ti distribution map measured by EDX. A local Pt mask was used for surface protection during preparation of the lamella by FIB.

solution. The EIS studies were performed with substrates that were obtained by anodizing at 20 V, 1 °C and sealed by ALD with a 50 nm nanolaminate (Fig. 5a) and with a 110 nm nanolaminate

(Fig. 5b). The EIS measurements were done after 0.5 h stabilization at OCP (denoted as “0 h”) and after 24 h immersion (denoted as “24 h”) in 0.5 M NaCl solution.

In the equivalent circuit model depicted in Fig. 5c, R.E. is the reference electrode, W.E. is the working electrode (the Al alloy),  $R_{\text{soln}}$  is the electrolyte resistance,  $R_c$  is the coating resistance,  $\emptyset$  marks constant phase element (CPE). The constant phase element considers the coating capacitance ( $C_c$ ), and exponent  $n$  is used in the calculation of the CPE. The exponent indicates the deviation of the insulator of a capacitor from an ideal dielectric behavior such that  $n = 1$  for an ideal capacitor and  $n = 0$  for an ideal resistor.<sup>33</sup>

EIS study results (Fig. 5) showed that the nanostructured coating prepared by sealing with 50 nm of nanolaminate was unstable, and at the end of the 24 h test the impedance  $|Z|$  had considerably decreased at lower frequencies  $f$  and no longer exhibited linear behavior (Fig. 5a). Furthermore, the  $\theta$ -curves, where  $\theta$  is phase angle depending on  $f$ , changed in shape and were near the  $90^\circ$  level only in a narrow high-frequency range. In contrast, the nanostructured coating formed on the Al alloy substrate by anodizing at 20 V,  $1^\circ\text{C}$  and sealed by ALD with 110 nm nanolaminate performed well in the EIS study, as the  $|Z|$ - and  $\theta$ -curves did not change during the 24 h immersion experiment (Fig. 5b). Furthermore, the impedance curve exhibited an almost linear behavior over the entire frequency range of  $2 \times 10^{-2}$ – $10^5$  Hz. The measured  $\theta$ -curve was also near the  $90^\circ$  level in a broad frequency range. To model the behavior of the better (second) coating depicted in Fig. 5b, a simpler ECM (Fig. 5c) with a single time constant was found to be adequate. As can be seen from Table II, the  $R_c$ ,  $C_c$ , and  $n$  values modelled for the second coating did not change after the 24 h immersion test, which confirms that the coating is chemically stable and free of major defects. Similar behavior and modelled ECM values were observed for a nanostructured coating in our previous paper,<sup>27</sup> where potentiodynamic anodizing in a three-electrode setup was used for pretreatment prior to sealing by ALD with 100 nm nanolaminate.

**Salt spray testing of nanostructured coatings.**—Salt spray testing was performed on eight substrates with different pre-treatments and coatings. The first substrate was polished and left bare (Fig. 6a). The second one was polished and anodized at 20 V,  $1^\circ\text{C}$ , but the AAO was not sealed (Fig. 6b). The third and fourth substrates were polished and coated by ALD at 50 nm (Fig. 6c) and 110 nm (Fig. 6d), respectively. The fifth and sixth substrates had a

nanostructured coating, which was prepared by anodizing the substrates first at 20 V,  $1^\circ\text{C}$  and then sealed by ALD with 50 nm (Fig. 6e) and 110 nm (Fig. 6f) nanolaminate. For comparison, the seventh substrate (Fig. 6g) was anodized at 20 V,  $1^\circ\text{C}$ , and then hydrothermally sealed by immersing the sample in boiling deionized water for 10 min. The eighth substrate (Fig. 6h) was anodized in 15% sulfuric acid at 20 V,  $23^\circ\text{C}$ , which was followed by sealing the pores with a commercial Rust Stop spray paint.<sup>34</sup>

Photos taken after the 1000 h salt spray test show severe damage to both polished and anodized substrates (Figs. 6a, 6b), where the latter exhibit slightly better performance. The polished substrates, which were coated with 50 and 110 nm nanolaminate, remained less damaged but had numerous small corrosion pits (Figs. 6c, 6d). Although the difference in performance between these two samples was not large, the polished Al alloy plate with a 110 nm coating had a smaller number of corrosion pits. In contrast, the anodized substrates that were sealed by ALD with a 50 nm (Fig. 6e) and a 110 nm nanolaminate (Fig. 6f) exhibited exceptional performance, with only two corrosion pits on the former sample (marked with red circles) and none on the latter sample. The Al alloy plate, which was anodized and then sealed by hydrothermal treatment (Fig. 6g), showed similar performance to that of the polished substrates, which were coated with nanolaminate, but had a much higher number of corrosion pits. Finally, the sample anodized at room temperature, which was sealed with commercial Rust Stop paint, remained unharmed during the salt spray test (Fig. 6h). The latter coating had a total thickness of 28–33  $\mu\text{m}$ ; thus, it was not a thin coating. The testing results show that the performance of the nanostructured coating developed in this work is comparable to that of commercial counterparts 10 times thicker, as well as with the thin nanostructured coating investigated in our first paper, where potentiodynamic anodization at room temperature was used for substrate pre-treatment.<sup>27</sup>

**STEM study of nanostructured coating.**—A lamella of the nanostructured coating was prepared by FIB for scanning transmission electron microscopy (STEM) studies from the sample that was prepared by anodizing the alloy at 20 V,  $1^\circ\text{C}$ , followed by sealing with 110 nm nanolaminate by ALD. The bright field STEM image of

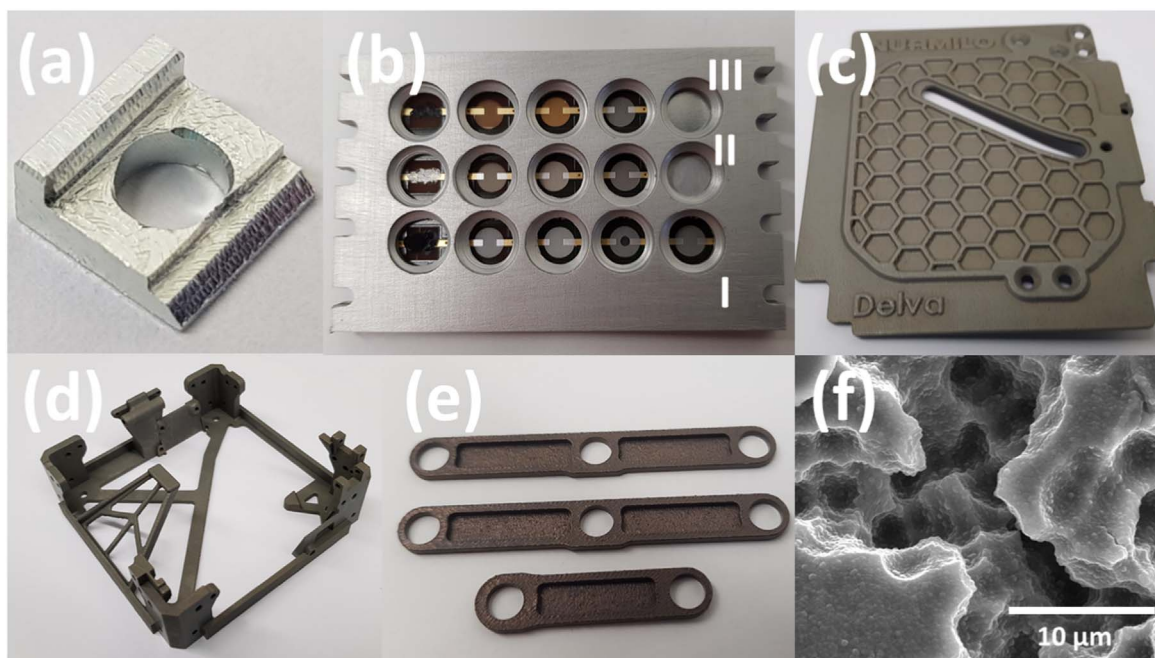


**Figure 9.** Use of nanolaminate and nanostructured coatings in space technology. Photos of satellite components (a)–(e) with nanolaminate (a) and nanostructured coating (b)–(e) that will be used on WISA Woodsat (a), (c)–(e) and ESTCube-2 (b). The surface of the nanostructured coating on 3D printed aluminum is depicted in an SEM image (f).

the lamella depicted in Fig. 7a shows individual layers of nanolaminate on the top part of the coating and a sealed AAO layer underneath it. However, a high-angle annular dark-field image of the same region depicted in Fig. 7b clearly shows the presence of a nanoscale structure. It should be noted that the lamella in the studied region has a uniform thickness, and the anodic aluminum oxide and atomic layer deposited aluminum oxide have the same or similar chemical composition. Further analysis of the lamella by mapping the distribution of elements with energy dispersive X-ray spectrometer (Figs. 7c–7h) shows that the AAO layer was depleted of Cu (Fig. 7f) during anodizing, which is in agreement with the SEM-EDX study depicted in Table SII in the Supplementary Material. The elemental maps also show the presence of sulfur in AAO owing to the use of sulfuric acid for anodizing the alloy (Table SII). According to the STEM-EDX study (Fig. 7h), sulfur is distributed uniformly in the AAO. However, it is no longer part of any reactive compound. After the end of the anodizing residual acid left in the pores reacts with the metal and/or oxide creating  $\text{Al}_2(\text{SO}_4)_3$ , thus it is not generating further corrosion. The STEM-EDX study also shows a region with a higher Mn content (Fig. 7g), which likely originates from an IMP that was not completely removed. However, the mean concentration of Mn in the coating measured in SEM-EDX studies is negligible (Table SII). Finally, the distribution of Ti (Fig. 7d) confirms that the nanostructured coating was prepared as intended, resulting in an AAO sealed mainly by  $\text{Al}_2\text{O}_3$  and having a top layer of nanolaminate.

**ATOX testing of nanostructured coating.**—The best-performing coating, which was prepared by anodizing at 20 V, 1 °C and sealed by ALD with 110 nm nanolaminate, was tested with a flux of energetic atomic oxygen at the LEOX facility of the European Space Research and Technology Centre. Visual observation of the sample before (Fig. 8a) and after (Fig. 8b) testing with atomic oxygen showed no obvious changes in the ceramic coating. However, the blue marker stripe seen in Fig. 8a was completely removed compared to the photograph taken after the test (Fig. 8b). The slight color difference of the samples was caused by different lighting conditions when taking the photos. Therefore, visual observation showed that exposure to atomic oxygen dramatically damaged a thin organic film, the stripe of a blue marker,<sup>35</sup> but the condition of the ceramic coating could not be evaluated.

A detailed HR-SEM study of the surface of an untested (Fig. 8c) and tested substrate (Fig. 8d) revealed that exposure to a flow of atomic oxygen caused a change in the surface morphology only at the nanoscale. Small grooves with a depth of  $\leq 10$  nm were formed on the surface of the tested substrate (Fig. 8d). HR-SEM studies also revealed that both the untested (Fig. 8c) and tested (Fig. 8d) substrates were sufficiently conductive for characterization by SEM. However, the surface of the tested substrate (Fig. 8d) could be slightly less conductive, which would enhance the image contrast, making it easier to characterize by SEM. Because the only conductive component in the coating is amorphous  $\text{TiO}_2$  prepared by ALD, it was necessary to study the change in detail.

Further HR-TEM analysis of a lamella prepared by SEM-FIB from the tested sample (Figs. 8e, 8f) did not show any changes in the top  $\text{TiO}_2$  layer of the nanolaminate (Fig. 8f). Thus, the precise cause of the change in the surface morphology of the tested sample is not clear. One possibility is the partial crystallization of the top  $\text{TiO}_2$  layer due to exposure to energetic atomic oxygen; however, TEM studies did not reveal nanocrystallites in the surface layer. Alternatively, the original  $\text{TiO}_2$  layer on top of the nanolaminate may be non-uniform in terms of mechanical properties, which could cause energetic atomic oxygen to sputter away the softer part of the titania topmost layer; however, both of these hypotheses are difficult to study in the TEM image because the upper part of the top layer was masked by platinum particles during the lamella preparation.

Because the coating suffered only minimal changes during the test with atomic oxygen while retaining its conductivity, it is likely

that the developed nanostructured coating is suitable for practical applications in low Earth orbit.

**Development and application of protective coatings for small satellites.**—Functional coatings of different thicknesses can be produced for aluminum alloys to significantly improve their performance. The developed coatings are particularly useful for satellite parts as they can be applied on substrates with complicated three-dimensional shapes without having a significant impact on their dimensions and weight. These coatings can be prepared by ALD and appropriate pre-treatments, including also conventional potentiostatic anodizing. Some examples of how these different types of coatings can be used are shown in Fig. 9.

On ESTCube-2, the nanostructured coating was applied to an aluminum  $65 \times 41 \times 3$  mm<sup>3</sup> cover panel (Fig. 9b, site I) of the materials testing module, which exposes the tested materials through holes (e.g., sites II and III) to atomic oxygen at a low Earth orbit. In this module, site II was used to test the nanostructured coating on a 0.1 mm foil, which was compared with the performance of an uncoated foil at site III. Visual inspection of the coated cover panel did not reveal any imperfections, and the sample looked similar to the AA2024-T3 sample with a nanostructured coating in the salt spray test (Fig. 6f).

On WISA Woodsat, a nanostructured coating was used on over 50 aluminum parts fabricated by 3D printing. These parts include panels (Fig. 9c), the main frame structure of the cube satellite (Fig. 9d), and parts of the mechanism (Fig. 9e) that extract the camera from the satellite to capture photos of its external surface while in orbit. In the extraction mechanism, a coating is used to mitigate cold welding in space. Assembly of the coated parts did not result in any loss of mobility. An additional SEM study of the surface showed that the coating was defect-free and followed the surface morphology of the 3D printed substrate (Fig. 9f).

## Discussion

**Choosing ALD process temperature and coating materials for protection of the Al alloy.**—The list of materials that could be used as an ALD protective coating for the Al-alloy is quite limited. Firstly, the temperature at which the coating is prepared must be relatively low,  $< 150$  °C not to decrease mechanical properties of the alloy.<sup>1–4,36</sup> Secondly, it is preferred that the corrosion protection coating is insulating and amorphous. Thirdly, since the metal precursor molecules must diffuse rapidly in and out of the AAO pores, the molecules need to be as small as possible. Fourthly, the precursors must be sufficiently reactive at low deposition temperatures but must not initiate corrosion of the metal substrate at the beginning of the process. Fifthly, for sealing the narrow and long pores of AAO and coating the samples with complex 3D geometry, it is not possible to increase the rate of the surface chemical reactions in ALD using plasma or other physical excitants. Sixthly, the cost of the precursors must be relatively low for the technology to be commercialize. All these conditions narrow the range of useful precursors/materials. We are currently not aware of any studies that use ALD coatings of materials other than alumina and/or titania to more or less successfully protect the Al2024 alloy. The  $\text{Al}_2\text{O}_3/\text{TiO}_2$  nanolaminates, that were first proposed by Matero et al. in 1999 for the protection of a steel,<sup>37</sup> and later investigated by other researchers on Al alloy substrates,<sup>23,27,28</sup> are also one of the best candidates used for sealing the AAO when preparing the new nanostructured coatings (Figs. 2, 3 and Table I). Because the benefits of  $\text{Al}_2\text{O}_3$  and  $\text{TiO}_2$  compensate the weaknesses of one another. For instance,  $\text{Al}_2\text{O}_3$  would normally gradually dissolve in aqueous medium but this is prevented by layers of  $\text{TiO}_2$ , which is chemically more stable.<sup>26</sup> Laminates and mixtures of ALD alumina and tantalum (V) oxide have also been used for the protection of a steel,<sup>38</sup> but tantalum (V) oxide is not as good an ion barrier as alumina and its precursor materials are more expensive than TMA. In this study,

alumina and titania were chosen because the materials and their precursors used fulfill all listed above conditions. Additionally, because alumina is a good insulator, ion barrier and suits chemically well with AAO, and titania grown at low temperature has a certain conductivity. Therefore, the conductivity of the coatings can be varied, which is important in many aerospace applications. The metal precursors, TMA and  $\text{TiCl}_4$  react well with  $\text{H}_2\text{O}$  also at low temperature, 125 °C,<sup>27,39</sup> and are relatively cheap. Finally, the laminate materials, alumina and titania are composed of light elements that will not emit significant hard X-ray fluorescence radiation due to cosmic particle/radiation bombardment in space (see also S3 in the Supplementary Material), so there is no additional threat to electronic components that could be shielded only by relatively thin Al-alloy walls.

**Additional aspects in the preparation of nanostructured coatings for the Al alloy.**—As expected, the properties of materials grown by ALD seem to carry over to the nanostructured coatings and affect their corrosion resistance, conductivity and hardness. For instance, in terms of corrosion resistance, the nanostructured coating with 110 nm nanolaminate (Figs. 5, 6) proposed in this study, is far superior to conventional ALD coatings on the Al alloy.<sup>23,24</sup> The highest hardness values were observed also for nanostructured coatings that were made by AAO sealing with  $\text{Al}_2\text{O}_3$  (Fig. 4, curve 4) or  $\text{Al}_2\text{O}_3/\text{TiO}_2$  nanolaminate (Fig. 4, curve 6), which is in good agreement with a previous study,<sup>28</sup> where the two aforementioned materials grown by ALD on Si substrate were harder than  $\text{TiO}_2$  and  $\text{Al}_2\text{O}_3\text{-TiO}_2$  mixture.

The nanostructured coating with ALD nanolaminate (Figs. 5, 6) developed in this study also seems to outperform other single and double-layered coatings prepared with the help of ALD by other research groups.<sup>23,24,37,38,40</sup> For instance, a double-layered coating made by combining sol-gel with ALD was far superior to only ALD coating but exhibited a dramatic rise in current densities already at mild anodic potentials in the LSV test.<sup>23</sup> A better performance was observed for a coating made by combining PVD with ALD, where the pitting potential was around 0.3 V.<sup>40</sup> In a later study performed by Härkönen et al., the best performing PVD + ALD coating exhibited notable signs of corrosion after 672 h neutral salt spray test.<sup>38</sup> In comparison, the nanostructured coating with nanolaminate investigated in this study has no signs of corrosion after 1000 h salt spray test (Fig. 6f) and exhibits no pitting in an LSV experiment up to 1 V (Fig. 3d, curve 4). Furthermore, the use of electrochemical pre-treatment and ALD allow applying the nanostructured coating on substrates that have a sophisticated three-dimensional shape, internal cavities or threads. As a rule, this is not possible for sol-gel (+ ALD) and PVD (+ ALD) coatings.

When comparing our nanostructured coatings with the earlier double deposition coatings obtained by the ALD method mentioned above, it is important to highlight the difference in the structure and, as a rule, in the thickness of these coatings. The earlier works were dealing with ALD thin films that were exploited for sealing defects in coatings made by other techniques (PVD, CVD, sol-gel method, etc).<sup>23,39</sup> In the electrochemical tests, the defects can be described as pores,<sup>24</sup> but no microscopic study has yet confirmed this. Thus, the defects could also be cracks due to mechanical stresses in relatively thick coatings that are more or less strait (Figs. 1d–1f) or growth defects due to any peculiarity of the substrate surface, etc. In current study, we first create an AAO via anodizing. The layer is chemically bonded to the substrate that gives best adhesion at the metal|oxide interface; the process also cleans and homogenizes chemically the surface. The AAO branching nanopores (Figs. 1b, 2a, 2e) are fully sealed, first, with the same Al-oxide and if having larger diameters then are following covered with other metal oxide layers, using for all ALD process (Figs. 1e, 1f)—this is principal difference between the thin nanostructured coating and mentioned above defect-sealed double coatings, which are as a rule thick coatings.

A crucial part of preparing nanostructured coatings is also anodizing, which creates the porous AAO layer. The latter usually

determines the final coating thickness, which depends on the application and is discussed in more detail in the next section. Based on our previous study<sup>27</sup> and the findings in this study we saw that potentiodynamic anodizing at room temperature (~22 °C) or potentiostatic anodizing at low temperature (1 °C) (Fig. 1), both result in well performing nanostructured coatings, although the radius of the AAO pores somewhat differs, but the branching structure remains. These results show that the proposed method for the preparation of nanostructured coatings can be quite versatile in terms of anodization and mainly depends on the ALD process used for the sealing. The ALD parameters has to be chosen carefully to maintain ALD mode growth, otherwise the branched pores could be easily clogged before the filling. Thus, an important aspect of anodizing is ensuring the reproducibility of the process, which requires a good control over the temperature of the electrolyte. We found that this could be achieved easily for small parts with an external ice bath around the anodizing bath. However, the most appropriate temperature control method is ultimately chosen by the user and depends on the application.

**Choosing the thickness of the nanostructured protective coating depending on the application.**—The thickness range of effective ALD based protective coatings for vulnerable to corrosion Al alloy AA2024 has to be discussed for two types of coatings. The first type are coatings that are deposited directly to the alloy substrate that has been polished and/or solvent cleaned, or on the alloy surface that is additionally electrochemically pre-treated at low potential. These coatings are as a rule <0.3  $\mu\text{m}$  thick and we classify them as ultra-thin coatings. The second type are the coatings that were deposited onto the anodized alloy substrate. These coatings have the thickness 0.5–3  $\mu\text{m}$  and we call them as thin coatings.

**The use of ultra-thin nanostructured coatings.**—The corrosion resistance of high precision and/or 3D printed aluminum alloy components can be significantly enhanced by coating them with the  $\text{Al}_2\text{O}_3/\text{TiO}_2$  nanolaminate via ALD. A 50–150 nm nanolaminate can be applied on the substrates in less than 6 h in our laboratory ALD reactor, but in a much shorter time in some new type reactors,<sup>41,42</sup> making it practical for industrial use in the near future. Generally, thorough cleaning with a mechanical surface finish and organic solvents is sufficient. It is important to note that in moist chloride-containing environments, the performance of the nanolaminate depends to some degree on the condition of the initial surface, exhibiting a coating efficiency between 0.35 in an earlier<sup>28</sup> and 0.68 in this study, see the latter in Table I. One possible reason for that could be different time interval between the substrate cleaning and ALD deposition, because of relatively fast start of local corrosion near the IMPs that are reaching the alloy surface.<sup>28</sup> The low potential electrochemical pretreatment can partly solve the problem. Therefore, electrochemical treatment at low potentials can improve the coating efficiency to 0.81.<sup>28</sup> However, it is not possible to completely remove large IMPs that are several micrometers in size. For that reason, nanostructured coatings deposited directly onto the ~20 nm thick oxide layer produced by the electrochemical pretreatment could fail in some of these locations, if working in harsh corrosive environments. At the same time, a rule of thumb is still that the smaller are the IMPs, the lower is the risk that the protective coating may fail—this is also a signal to the alloy manufacturers on how to improve the alloy.

Otherwise, the nanolaminate is chemically stable in water<sup>28</sup> and suffers little damage from the direct flux of atomic oxygen (Fig. 8), which makes the coating a good choice for protecting materials against corrosion in terrestrial and space applications. An example of using the nanolaminate is shown in Fig. 9a, where the high-precision aluminum substrate is only a few millimeters in size and in direct contact with another metal after assembly, which increases the risk of galvanic corrosion due to potential difference. Because of the small size of such substrates, hundreds of them can be coated simultaneously during the ALD process in a commercial reactor,

which greatly improves their performance at a very low increase in cost per item.


*The use of thin nanostructured coatings.*—If the nanolaminate is insufficient for high-performance applications, and the sample dimension tolerances are not so critical, then a sub-micrometric nanostructured coating can be considered, which is mechanically more durable and provides excellent protection against corrosion. Such a coating can be achieved using a carefully controlled electrochemical pre-treatment at anodic potentials to create a sub-micrometric porous AAO layer, which is then sealed by ALD with the nanolaminate, see cross-sections in Figs. 1b, 1d, and in Fig. 7c in an earlier study.<sup>27</sup> This process may require more stringent pretreatment checks, but the resulting coating is defect-free and has an efficiency of 1.0. Which is particularly useful for mitigating galvanic corrosion on high-precision components, where the dimensional tolerances are less than a micron. It is worth mentioning that anodizing increases the sample dimensions by about 50% of the AAO thickness.<sup>2</sup>

In applications where the dimensional tolerance is 1–5  $\mu\text{m}$  or greater, nanostructured coatings can be prepared using conventional potentiostatic anodizing for pre-treatment prior to sealing by ALD with a suitable material. In this study, we demonstrated how anodizing at 10 V, 1 °C, and 20 V, 1 °C can be used to prepare nanostructured coatings with thicknesses  $\sim 1$  and 2–4  $\mu\text{m}$ , respectively (Fig. 2). This anodizing process also benefits from a simple method of temperature control, where an external ice bath was used to keep the electrolyte around 1 °C and ensure stable parameters during anodization of several batches of substrates. The choice of material used for sealing by ALD allows the modification of the properties of the nanostructured coating. For instance, insulating coatings are achieved by sealing AAO with  $\text{Al}_2\text{O}_3$ , which is beneficial for creating a dielectric barrier or simply a hard surface. Alternatively, sealing the nanoscale pores of AAO with  $\text{Al}_2\text{O}_3$  and applying a nanolaminate on top will result in a nanostructured coating, which benefits from its dielectric properties and hardness while also providing additional chemical stability for use in moist environments, and a semiconductive surface to mitigate charging in space. If it is necessary to create a more conductive coating overall, then the nanoscale pores in the AAO can be sealed by ALD with  $\text{TiO}_2$  instead of  $\text{Al}_2\text{O}_3$ . The only possible disadvantage of using potentiostatic anodization at low temperatures for pre-treatment may be the creation of cracks in the AAO layer and limited dissolution of the IMP leftovers. In our study, we mitigated this possible issue by sealing the AAO with 20 nm of  $\text{Al}_2\text{O}_3$  and then coating the entire surface with an additional 90 nm of nanolaminate. This type of nanostructured coating was also used to cover the satellite parts depicted in Figs. 9b–9e for different purposes.

### Acknowledgments

The authors would like to acknowledge the Estonian Ministry of Education and Research by granting the projects IUT2–24, TLTFY14054T, PSG448, PRG4, SLTFY16134T and by the EU through the European Regional Development Fund under project TK141 (2014-2020.4.01.15-00). The atomic oxygen testing was performed in the framework of the “Announcement of opportunity for atomic oxygen in the ESTEC Materials and Electrical Components Laboratory/ESA-TECQE-AO-013375,” through a collaboration with Picosun Oy. The authors also thank Dr. Elo Kibena-Pöldsepp for the electrodeposition of Ag onto the anodized substrates.

### ORCID

Lauri Aarik  <https://orcid.org/0000-0002-7785-1351>  
 Jekaterina Kozlova  <https://orcid.org/0000-0002-7775-1246>  
 Aivar Tarre  <https://orcid.org/0000-0003-1518-2989>  
 Väino Sammelselg  <https://orcid.org/0000-0002-3598-9184>

### References

1. C. R. Brooks, *Heat Treatment, Structure and Properties of Nonferrous Alloys* (American Society for Metals, Metals Park, Ohio) p. 121 (1982).
2. J. R. Davis, *Aluminum and Aluminum Alloys* (ASM International, Materials Park, OH, USA) ASM Specialty Handbook., (1993), and Davis J.R., *Corrosion of Aluminum and Aluminum Alloys* (ASM International, Materials Park, OH, USA) ASM Specialty Handbook. (1999); and Kaufman G., *Corrosion of Aluminum and Aluminum Alloys*. In: *Corrosion: Materials*, Cramer, S.D. and Covino B.S. Jr. (Eds.) (ASM International, OH, USA), 95 (2005).
3. K. H. Matucha, “Structure and properties of nonferrous alloys.” *Mater. Sci. Technol.* (Weinheim Publisher, New York, NY) 8, 213 (1996).
4. G. E. Totten and D. Scott MacKenzie, *Handbook of Aluminum, volume 2, Alloy production and Materials Manufacturing* (CRC Press, New York, NY) (2003).
5. [dataset] Material Property Data (ASM MatWeb), <http://asm.matweb.com/search/SpecificMaterial.asp?bassnum=MA2024T3>, and (<http://matweb.com/search/DataSheet.aspx?MatGUID=781ce4db30c4d548320b0ab262a5d28>); last visited in June 2022.
6. B. D. Dunn, *The Corrosion Properties of Spacelab Structural Alloy Aluminum 2219-T851 (ESA STR-212)*. (ESA Communication Production Office, ESTEC, Noordwijk, The Netherlands) (1984), [http://esmat.esa.int/Publications/Published\\_papers/ESA\\_STR-212.pdf](http://esmat.esa.int/Publications/Published_papers/ESA_STR-212.pdf); last visited in June 2022.
7. A. M. Pereira, G. Pimenta, and B. D. Dunn, *Assessment of Chemical Conversion Coatings for the Protection of Aluminum Alloys A Comparison of Alodine 1200 with Chromium-Free Conversion Coatings (ESA-STM-276, 2008)*. (ESA Communication Production Office, ESTEC, Noordwijk, The Netherlands).
8. EU hydrogen policy. Hydrogen as an energy carrier for a climate-neutral economy, [https://europa.eu/RegData/etudes/BRIE/2021/689332/EPRS\\_BRI\(2021\)689332\\_EN.pdf](https://europa.eu/RegData/etudes/BRIE/2021/689332/EPRS_BRI(2021)689332_EN.pdf); last visited in June 2022.
9. S. Kramer and D. Mosher. Here’s how much money it actually costs to launch stuff into space, Tech Insider, <https://businessinsider.com/spacex-rocket-cargo-price-by-weight-2016-6>; last visited June 2022.
10. O. Zeynali, D. Masti, and S. Gandomkar, *Adv. in Appl. Sci. Research*, 3, 446 (2012), (<https://www.primescholars.com/articles/shielding-protection-of-electronic-circuits-against-radiation-effects-of-spacehigh-energy-particles.pdf>); last visited in June 2022.
11. A. Boag, A. E. Hughes, N. C. Wilson, A. Torpy, C. M. MacRae, A. M. Glenn, and T. H. Muster, *Corros. Sci.*, 51, 1565 (2009).
12. A. Boag, A. E. Hughes, A. M. Glenn, T. H. Muster, and D. McCulloch, *Corros. Sci.*, 53, 17 (2011).
13. A. E. Hughes, A. Boag, A. M. Glenn, D. McCulloch, T. J. Muster, C. Ryan, C. Luo, X. Zhou, and G. E. Thompson, *Corros. Sci.*, 53, 27 (2011).
14. A. M. Glenn, T. H. Muster, C. Luo, X. Zhou, G. E. Thompson, A. Boag, and A. E. Hughes, *Corros. Sci.*, 53, 40 (2011).
15. A. Merstallinger, M. Sales, E. Semerad, and B. D. Dunn, “Assessment of Cold Welding Between Seperable Contact Surfaces Due to Impact and Fretting Under Vacuum.” *Materials Science* (European Space Agency, Noordwijk, Netherlands) European Space Agency Scientific and Technical Reports, STM-279 (2009).
16. S. Borenstein, (2022), Phys.org, <https://phys.org/news/2009-05-stuck-dead-battery-bedevel-hubble.html> Stuck bolt, dead battery bedevil Hubble repairs; last visited in June 2022.
17. A. de Rooij, “Corrosion in Space.” *Encyclopedia of Aerospace Engineering*, ed. R. Blockley and W. Shyy (Wiley, <https://onlinelibrary.wiley.com/>) (2010), [https://onlinelibrary.wiley.com/doi/abs/10.1002/9780470686652.eae242http://esmat.esa.int/publications/published\\_papers/corrosion\\_in\\_space.pdf](https://onlinelibrary.wiley.com/doi/abs/10.1002/9780470686652.eae242http://esmat.esa.int/publications/published_papers/corrosion_in_space.pdf); last visited in June 2022..
18. K. K. de Groh, B. A. Banks, J. A. Dever, D. A. Jaworske, S. K. Miller, E. A. Sechkar, and S. R. Panko, NASA Glenn Research Center’s Materials International Space Station Experiments (MISSE 1–7). NASA/TM–2008-215482, published under NASA Glenn Research Center’s Materials International Space Station Experiments (MISSE 1-7) - NASA Technical Reports Server (NTRS): Microsoft Word - E-16690TM.doc (nasa.gov); last visited in June 2022.
19. D. R. Gabe, *Met. Finish.*, 100, 52 (2002).
20. A. D. Juhl, *Met. Finish.*, 108, 20 (2010).
21. S. Shrestha and B. D. Dunn, “Advanced plasma electrolytic oxidation treatment for protection of light weight materials and structures in a space environment.” *Advanced Surface Treatment*. (European Space Agency, Noordwijk, Netherlands) (2022), can be found under ([http://esmat.esa.int/Publications/Published\\_papers/Keronite2007paper.pdf](http://esmat.esa.int/Publications/Published_papers/Keronite2007paper.pdf)); last visited in May 2022.
22. M. Ritala and M. Leskelä, “Atomic layer deposition.” *Handbook of Thin Films*, 1, 103 (2002).
23. E. Marin, A. Lanzutti, F. Andreatta, M. Lekka, L. Guzman, and L. Fedrizzi, *Corros. Rev.*, 29, 191 (2011).
24. S. E. Potts et al., *J. Electrochem. Soc.*, 158, C132 (2011).
25. V. Sammelselg, L. Aarik, and M. Merisalu, WO 2014102758 A1 (2012), EP 2 938 758 B1 (2016), US 9,834,849 B2 (2017), JP 63336477 B2 (2018).
26. V. Sammelselg, I. Netšipailo, A. Aidla, A. Tarre, L. Aarik, J. Asari, P. Ritslaid, and J. Aarik, *Thin Solid Films*, 542, 219 (2013).
27. M. Merisalu, L. Aarik, J. Kozlova, H. Mändar, A. Tarre, and V. Sammelselg, *Surf. and Coat. Technology*, 411, 126993 (2021).
28. M. Merisalu, L. Aarik, J. Kozlova, H. Mändar, A. Tarre, H. M. Piirsoo, and V. Sammelselg, *Surf. and Coat. Technology*, 435, 128240 (2022).
29. J. Aarik, A. Aidla, A. Kasikov, H. Mändar, R. Rammula, and V. Sammelselg, *App. Surf. Sci.*, 252, 5723 (2006).
30. R. Ali, M. R. Saleem, P. Pääkkönen, and S. Honkanen, *Nanomaterials*, 5, 792 (2015).

31. Testing of materials with atomic oxygen at the Low Earth Orbit Facility (LEOX), [https://esa.int/Enabling\\_Support/Space\\_Engineering\\_Technology/Atomic\\_oxygen\\_generator\\_simulates\\_fire\\_in\\_the\\_sky](https://esa.int/Enabling_Support/Space_Engineering_Technology/Atomic_oxygen_generator_simulates_fire_in_the_sky); last visited in June 2022.
32. Y. Zhang, J. A. Bertrand, R. Yang, S. M. George, and Y. C. Lee, *Thin Solid Films*, **517**, 3269 (2009).
33. P. Zoltowski, *J. Electroanal. Chem.*, **443**, 149 (1998).
34. Rust Stop paint, <https://motipdupli.com/en/products/dupli-color/rust-protection/rust-stop/ipg-1270/tm-1270.html>; last visited May 2022..
35. CompoundChem, Chemical composition of highlighter colors, can be found under; last visited in June 2022, <https://compoundchem.com/2015/01/22/highlighters>.
36. Data from a private industrial partner.
37. R. Matero, M. Ritala, M. Leskelä, T. Salo, J. Aromaa, and O. Forsen, *J. Phys. IV France*, **9**, 493 (1999).
38. E. Härkönen et al., *ACS Appl. Mater. Interfaces*, **6**, 1893 (2014).
39. S. M. George, *Chem. Rev.*, **110**, 111 (2010).
40. E. Marin, L. Guzman, A. Lanzutti, L. Fedrizzi, and M. Saikkonen, *Electrochem. Commun.*, **10**, 2060 (2009).
41. P. Poedt, A. Lankhorst, F. Roozeboom, K. Spee, D. Maas, and A. Vermeer, *Adv. Mater.*, **22**, 3564 (2010).
42. D. Muñoz-Rojas, T. Mairdron, A. Esteve, F. Pierrat, J. C. S. Kools, and J.-M. Decams, *Mater. Today Chem.*, **12**, 96 (2019).